Unidirectional freezing as a tool for tailoring air permeability in macroporous poly(ethylene glycol)-based cross-linked networks

Walter F. Schroeder, Roberto J. J. Williams, Cristina E. Hoppe & Hernán E. Romeo

Journal of Materials Science
Full Set - Includes `Journal of Materials Science Letters'

ISSN 0022-2461
Volume 52
Number 23

J Mater Sci (2017) 52:13669-13680
DOI 10.1007/s10853-017-1460-4

Springer

J Mater Sci (2017) 52:13669–13680

Polymers

Unidirectional freezing as a tool for tailoring air permeability in macroporous poly(ethylene glycol)-based cross-linked networks

Walter F. Schroeder[1], Roberto J. J. Williams[1], Cristina E. Hoppe[1], and Hernán E. Romeo[1,*]

[1] *Institute of Materials Science and Technology (INTEMA), University of Mar del Plata (UNMdP) and National Research Council (CONICET), Juan B. Justo 4302, Mar del Plata, Argentina*

Received: 3 July 2017
Accepted: 7 August 2017
Published online: 16 August 2017

ABSTRACT

Unidirectional freezing followed by photopolymerization at subzero temperatures was used to obtain highly air-permeable monoliths with ordered porous structures. Scaffolds were obtained from aqueous solutions of a poly(ethylene glycol)dimethacrylate (PEGDMA) oligomer, a photosensitizer and a reducing agent. Solutions were vertically frozen in liquid nitrogen at a controlled rate to induce the oriented growth of ice crystals and then cryo-photopolymerized under blue-light irradiation. Ice crystals were finally removed under vacuum producing macroporous hydrophilic networks with aligned pores. Porosities ranged between 80 and 95%, depending on the initial concentration of PEGDMA. The influence of processing variables on the final properties of the materials was addressed, concerning particularly the effect of porosity and freezing directionality on air permeability. Compared to porous PEGDMA-based monoliths with non-aligned macropores, gas permeability was two to three times higher for oriented scaffolds at the same porosity level, a fact explained by the easier transport of gas molecules through the aligned structures. However, the role of pore orientation on gas permeability was shown to be less marked as porosity increased. The results demonstrate that the use of unidirectional freezing strongly increases the permeability of monolithic samples up to values usually required, for instance, in tissue engineering applications (higher than 2D). These findings provide new perspectives on pore design principles toward future scaffolding of polymeric cross-linked matrices.

Address correspondence to E-mail: hromeo@fi.mdp.edu.ar

DOI 10.1007/s10853-017-1460-4

Introduction

With the current focus put on actual applications, the requirement for non-toxic, economical and scalable routes for the synthesis of macroporous materials with specific morphologies and elevated tunability is continuously rising. Particularly, macroporous polymeric hydrogels have become interesting candidates for the development of new materials and devices, especially in the fields of biomedicine, biotechnology and separation science [1–7]. Poly(ethylene glycol) (PEG)-based hydrogels have been recognized as especially adequate platforms for this type of applications, due to its excellent biocompatibility, high hydrophilicity and outstanding resistance to protein adhesion [8–10].

The inclusion of porosity in polymeric materials constitutes the central challenge for the fabrication of a number of technologically relevant materials, ranging from polymeric sponges for the cleaning of oil spills [11–13] to 3D phantoms for medical research [14]. A variety of techniques have been developed to introduce porosity in bulk materials, including phase separation [15], ice drying [16], gas foaming [17] and the use of porogens [18] or high internal phase emulsions (HIPEs) [19–21], among others. In most of these approaches, macroporous materials with randomly oriented porosities are obtained. However, some applications specifically require oriented porosity along one direction. This is especially crucial in the development of some tissue engineering scaffolds [22], separation columns [6] or actuators requiring an anisotropic response [23, 24]. It is in this field that the directional freezing technique has become the option of choice. In this approach (typically referred to as ISISA/ice-segregation-induced self-assembly), water-based solutions/dispersions are frozen by imposing a strong temperature gradient across the sample [25, 26]. Under such conditions, ice crystals grow up driven by the temperature gradient, which triggers the segregation of solutes from the aqueous phase. The confinement and consequent rise in concentration of the expelled solutes between the oriented crystals lead to their final self-assembly. The subsequent removal of ice crystals (via freeze-drying) leads to the formation of oriented porous structures with macrochannels longitudinally aligned along the sample [27]. The problem associated with hydrogels, and other non-soluble cross-linked materials, is the probability of fracture and structure disruption that can occur during ice crystallization. A much better control of porosity and pore size could be attained if freezing is applied on the starting monomer solution, previous to the polymerization and network formation. Some examples using this last approach can be found in the literature, most of them based on the freezing of non-aqueous solutions of polymer precursors [28–30] followed by photoirradiation with UV light [28, 29]. However, in spite of these successful examples, it is clear that easy procedures combining low-cost, low energy consumption setups and non-toxic approaches toward macroporous PEG hydrogels with aligned channels and well-tuned properties have to be developed. In this last sense, the directional freezing technique can be further exploited toward the desired goal, doing more than simply allow aligning pores in a polymeric matrix. Depending on both the imposed freezing conditions and concentrations used in the starting solutions, it is possible to modulate not only the pore size of the materials, but also tuning the effective morphology of the growing ice crystals and, thus, of the oriented macropores [25, 26]. This modulation of pore identity is one of the most powerful tools we count with, exerting a strong influence on the final properties of the polymeric scaffolds, mainly on those related to transport phenomena associated with the porous architecture.

In this work, we present a strategy to obtain PEG-based hydrogels with oriented macroporosity based on the unidirectional freezing of aqueous solutions of poly(ethylene glycol)dimethacrylate (PEGDMA) oligomers followed by fast cryo-photopolymerization with visible light. Final porous scaffolds are obtained by simply freeze-drying the irradiated frozen monoliths. Influence of processing variables on the final properties of the materials is especially addressed, particularly which concerns to the effect of porosity and freezing directionality on air permeability. The possibility of easily tuning gas permeability of macroporous polymers has been recognized as a technological advantage, especially in applications in which this property is of paramount importance, like tissue engineering or gas separation processes [21]. Recently, Seuba et al. [31] demonstrated that modification of the experimental parameters enables controlling the microstructure of ceramic monoliths obtained by ice-templating, allowing tailoring,

independently, their mechanical and gas flow properties. Here we demonstrate that structural modifications induced on macropore walls via a rational use of directional freezing lead to significant variations in air permeability of PEG-based hydrogels cryo-photopolymerized with visible light. In order to assess the effect of pore orientation on effective air permeability, porous PEG hydrogels with non-oriented macropores were also synthesized and tested. Permeabilities as high as 2.4D are easily attained as a consequence of cryogenically induced morphological variations under directional processing. The findings reported here provide new perspectives on pore design principles toward future scaffolding of porous polymeric cross-linked matrices.

Materials and methods

Materials

Poly(ethylene glycol)dimethacrylate (PEGDMA, $M_n = 500$), camphorquinone (CQ) and ethyl-4-dimethyl aminobenzoate (EDMAB) were purchased from Aldrich and used without further purification.

Methods

Photopolymerization of PEGDMA

Formulations of PEGDMA containing 2 wt% CQ as photosensitizer and 2 wt% EDMAB as reducing agent (both respect to PEGDMA), were sandwiched between two glass plates separated by a 0.5-mm copper spacer ring. The setup was placed in a freezing stage (THMS600, Linkam) with programmable temperature control (TMS 93 Series, Linkam), mounted in the holder of a Nicolet 6700 Thermo Scientific FTIR spectrometer. Irradiation was performed with a light-emitting diode (LED), at a wavelength range 410–530 nm and an irradiance of 600 mW/cm^2 (measured with potassium ferrioxalate as actinometer). Photopolymerizations were carried out at 20, −5, −15 and −30 °C. The evolution of conversion was determined by regular measurements of the intensity of the methacrylate absorption band located at 6165 cm^{-1} (=CH_2 first overtone), employing an FTIR device. Spectra were acquired in the transmission mode, in the 4000–7000-cm^{-1} range from 32 co-added scans at 4 cm^{-1} resolution.

Thermal properties of the oligomer and the polymer network

Differential scanning calorimetry (DSC, PerkinElmer Pyris 1) was employed to determine the location of the melting peak of the PEGDMA oligomer and the glass transition temperature (T_g) of the polymer network with full conversion of methacrylate groups. Scans were performed at 10 °C/min under nitrogen flow. The T_g was defined at the onset of the change in specific heat.

Preparation of cryogels with aligned or non-aligned macropores

Solutions of PEGDMA, CQ (2 wt%) and EDMAB (2 wt%) (both respect to PEGDMA) in water were prepared. In order to produce a significant morphological variation on pore wall features during the directional freezing, two water concentrations were used: 80 and 95 wt% with respect to PEGDMA. These extremes were tested to modify the PEGDMA concentration in the starting solutions. Monomer concentration is known to control solution viscosity, diffusivity conditions and, consequently, the degree of supercooling in the freezing solution [32]. Accordingly, monomer concentration would exert changes in pore wall identity, from smooth to dendrite-like morphologies as concentration increases.

The prepared water-based solutions were poured into insulin syringes (80 mm length, 4.5 mm diameter) and dipped into liquid nitrogen (−196 °C) at a controlled immersion rate (5 mm/min). In order to evaluate the effect of pore orientation on air permeability, porous PEGDMA-based monoliths with non-aligned macropores were also synthesized. For this, aqueous solutions with the same concentrations used in the directional freezing process were poured into insulin syringes and frozen in liquid nitrogen, but this time via a sudden immersion. After complete freezing of all samples, syringes were transferred to a chamber at −15 °C. After holding samples for 10 min at this temperature, visible-light irradiation was performed for 40 min with the same LED setup used in the polymerization of pure PEGDMA. Every 10 min the syringe was rotated 90° to produce a uniform polymerization. Monoliths were recovered by breaking the syringes after freeze-drying the samples for 48 h using a VirTis Benchtop SLC (2KBTES-SS) freeze-drier. The resulting cross-linked

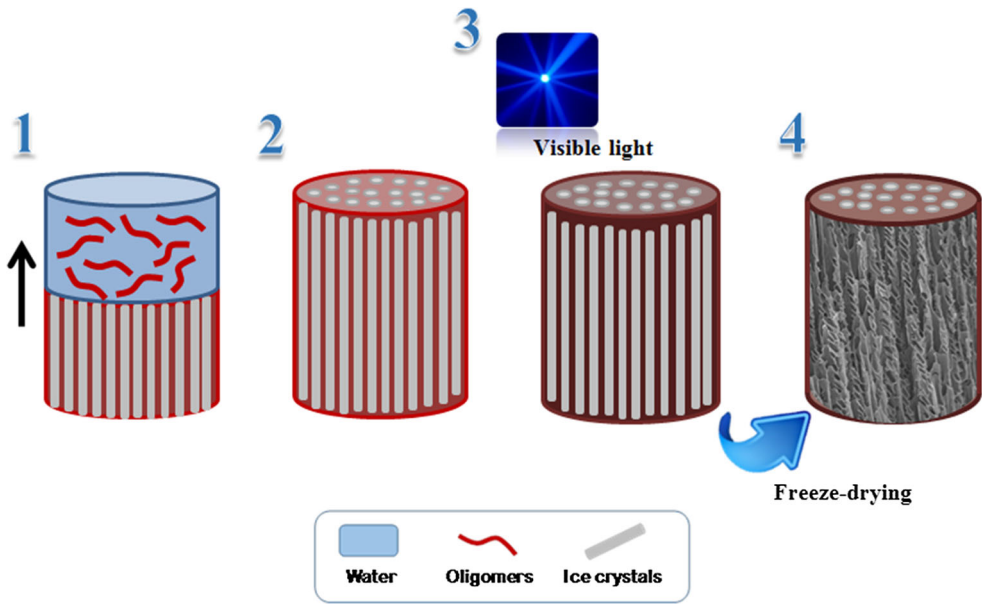

Figure 1 Scheme of a porous monolithic cryogel obtained by unidirectional freezing followed by cryo-photopolymerization: *1* vertical growing of ice crystals. The monomer/oligomer is segregated by, and trapped between, the ice crystals. The *arrow* indicates the freezing direction. *2* Directional immersion proceeds until the whole system is frozen. Ice crystals act as pore templates, *3* once frozen, the system is irradiated at subzero temperature to polymerize the trapped monomer/oligomer (in our case blue light was used), *4* after freeze-drying, a macroporous scaffold with aligned channels is obtained.

porous monoliths kept both the size and shape of the syringes. Overall conversions of PEGDMA were determined by the intensity of the methacrylate band at 6165 cm^{-1} with material taken from the transversal section of the monolithic samples. Figure 1 shows a schematic representation of the unidirectional process followed by the cryo-photopolymerization approach, leading to a cryogel with aligned macropores.

Characterization of the monoliths

To avoid end effects, cylinders of lengths in the range 1–2.5 cm were cut from the middle part of both types of monoliths (with aligned or non-aligned pores). Porous structures were observed by scanning electron microscopy (SEM) of metalized samples, using a JEOL JXA-8600 instrument.

Porosities of monoliths were determined from their bulk densities ρ_b (g/cm^3), calculated from the weights and geometrical volumes, and the density of the polymer network taken as the one of the polyethylene glycol (1.13 g/cm^3). Porosities ($\varepsilon\%$) were calculated as

$$\varepsilon\% = [1 - (\rho_b/1.13)] \times 100 \quad (1)$$

The air permeability of monoliths with different lengths (L) was measured with a homemade device (Fig. 2).

A glass ampoule ($V = 190$ cm^3) was joined to a manometer and to a two-way glass valve connected either to a vacuum line or to a rubber tube closed with an inserted monolith wrapped with Teflon®. The ampoule was first evacuated, the valve was turned to connect the rubber tube, and the increase in pressure (p) was followed in time (t). It was previously confirmed that when the porous monolith was replaced by a non-porous cylinder of the neat polymer network wrapped with Teflon®, vacuum was maintained. Therefore, the increase in pressure was produced by the flow of air through the porous samples.

The value of permeability (B) was obtained from Darcy's law, relating the flux of air (taken as a pseudo-component) with the pressure gradient along the axial direction z:

$$N = -B(p/\mu R_g T)\,(dp/dz) \quad (2)$$

In Eq. (2), N is expressed in moles per unit area and time; μ is the viscosity of air, R_g is the gas constant, and T is the absolute temperature. Dimensions of B are m^2 or millidarcys (mD) (1 mD = 0.987×10^{-15} m^2).

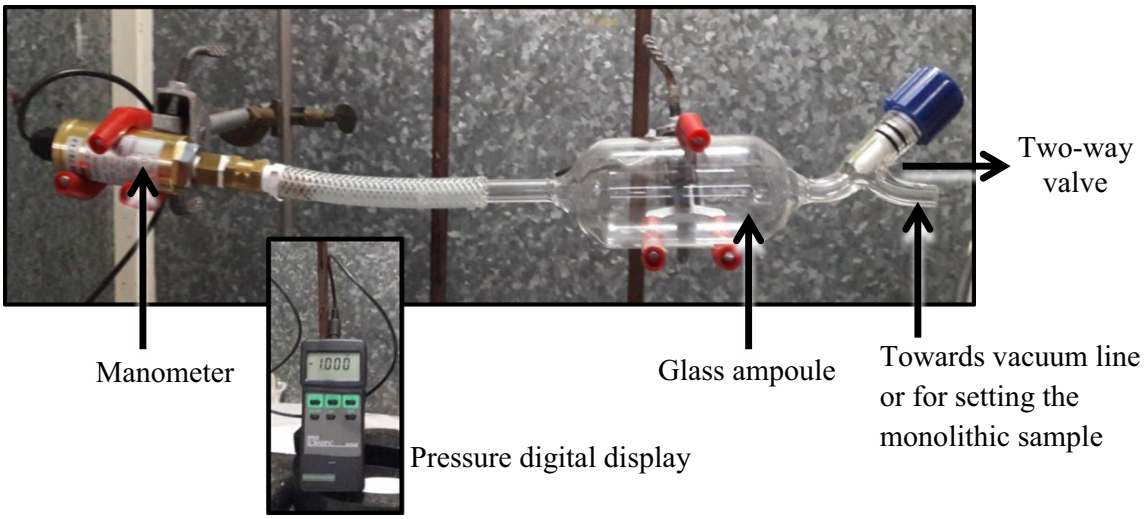

Figure 2 Picture of the homemade device employed to determine the air permeability of monoliths.

A pseudo-steady state is rapidly attained where the air flux depends on time, but it does not vary in the axial direction of the monolith; e.g., N does not depend on z. Equation (2) may be integrated under this condition to give:

$$N = \left(B/\mu R_g T\right)\left(p_0 + p\right)\left(p_0 - p\right)/2L \quad (3)$$

In Eq. (3), p_0 is the atmospheric pressure.

The instantaneous value of the air flux can be related to the derivative of pressure with time, employing the ideal gas law:

$$N = \left(V/R_g TA\right)\mathrm{d}p/\mathrm{d}t \quad (4)$$

A is the transversal area of the monolith.

Equating Eqs. (3) and (4) and integrating lead to:

$$\ln\left[\left(p_0 + p\right)/\left(p_0 - p\right)\right] = \left(BAp_0/\mu LV\right)t \quad (5)$$

The permeability was finally obtained from the slope of the linear plot of the left-hand side of Eq. (5) with respect to time. The linearity also proves the validity of Darcy's law in the range of experimental values of fluxes. Notice that the experimental method is robust in the sense that if the initial flux were too high to verify Darcy's law, its continuous decrease would necessary lead to a p versus t region where the law is valid.

Results and discussion

Analysis of the PEG-based reactive system

The proposed strategy for the synthesis of PEG-based cross-linked macroporous scaffolds with aligned pores is based on the directional freezing of a PEG-based precursor dissolved in water followed by its subsequent polymerization at subzero temperatures under low energy conditions (visible-light source by LED illumination). A commercially available poly (ethylene glycol)dimethacrylate oligomer (PEGDMA, $M_n = 500$) was selected as an adequate building block for this approach. This oligomer has two characteristics that make it desirable as a precursor: (1) its high solubility in water in a wide range of compositions and (2) the possibility of being mixed with a photosensitizer and a reducing agent for being rapidly photopolymerized with visible light at subzero temperatures. Photoinduced reactions have proved to be of paramount importance in a variety of technological applications (adhesives, coatings, photolithography) [33]. In particular, the free radical photopolymerization of acrylate/methacrylate monomers is an attractive path for the synthesis of cross-linked matrices at both low temperatures and humid environments (as those required in this approach), conditions under which other polymerizing mechanisms would be completely unfeasible. The possibility of polymerizing the precursor in a humid environment enables its homogeneous processing by ice-templating, which is a required condition for the controlled tuning of the final pore morphology. On the other hand, the use of a temperature below 0 °C allows avoiding melting of the ice crystals, which would disrupt the organization achieved by ice-templating. In this work, visible-light photopolymerization was triggered by the addition of

camphorquinone (CQ) as a photosensitizer and ethyl-4-dimethyl aminobenzoate (EDMAB) as a reducing agent. The initiating mechanism has been proposed in the literature and is briefly described here [33]. Irradiation with visible light produces the excitation of CQ to its singlet state, which is rapidly converted to its triplet state by intersystem crossing. The excited CQ molecule is subsequently reduced by EDMAB to generate ketyl and α-amino free radicals. It is considered that the α-amino radicals are responsible for initiating the polymerization, whereas the ketyl radicals are not efficient initiators and finally dimerize.

A series of initial studies on the PEGDMA oligomer were carried out in order to analyze the best conditions to achieve the desired goal. First of all, and before carrying out the reaction in the presence of water, the effect of temperature on the photopolymerization rate of the oligomer in bulk was examined. Figure 3 shows the DSC heating curve for the pure PEGDMA precursor.

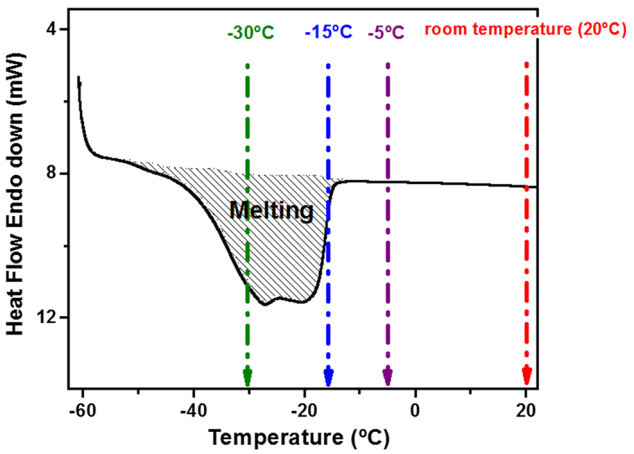

Figure 3 DSC scan of the oligomer (PEGDMA) showing a broad endotherm corresponding to the melting of PEG crystals.

The melting of PEGDMA crystals appears as a wide endothermic peak (from −52 to −13 °C). Therefore, polymerizations at temperatures below −13 °C would not reach full conversion because of the residual fraction of crystallized monomer. On the other hand, the glass transition temperature (onset value) of the fully cross-linked polymer network was −32 °C (Fig. S1), meaning that polymerization of the amorphous fraction of monomer below this temperature would be arrested by vitrification. Hence, four temperatures were selected for analyzing the visible-light polymerization of PEGDMA: −30, −15, −5 and 20 °C. Figure 4a illustrates the decrease in the intensity of the band corresponding to methacrylate groups in FTIR spectra during photopolymerization at 20 °C, whereas Fig. 4b shows the evolution of conversion at the four selected temperatures.

As can be seen, the polymerization rate of PEGDMA is strongly dependent on the reaction temperature. While complete conversion was achieved after 2-min irradiation at 20 °C, the polymerization rate became diffusion-limited at lower temperatures. Conversion reached values of 0.8 at −5 °C, 0.77 at −15 °C and 0.46 at −30 °C, after 7-min irradiation. For cross-linking free radical

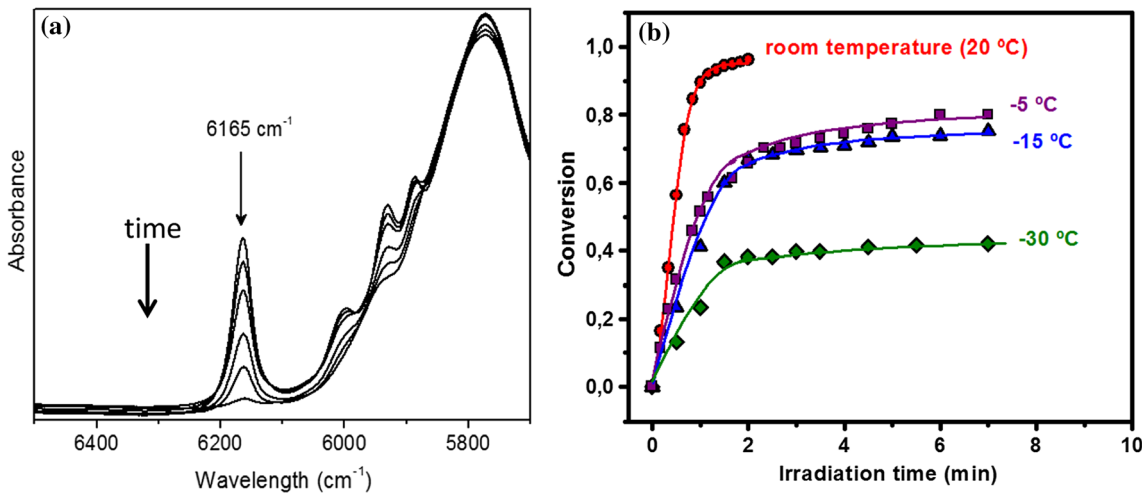

Figure 4 PEG-based reactive system in the absence of water. **a** Evolution of the intensity of the band of methacrylate groups in FTIR spectra during photopolymerization at 20 °C (time interval for the measurement: 2 min). **b** Evolution of the conversion of PEGDMA oligomer as a function of the irradiation time for the four selected temperatures.

polymerizations, the reaction rate decreases in the diffusion-limited regime due to two main effects [34]: a decrease in initiator efficiency and the trapping of radicals in the network. Because radical trapping is dependent on segmental mobility of the network, lower curing temperatures move the onset of trapping to lower conversions. In fact, the onset of radical trapping may be simultaneous with the decreasing initiator efficiency, since both are diffusion-limited phenomena on roughly the same molecular scale [35]. In addition, the presence of crystallized oligomer below −13 °C reduces even more the ultimate degree of cure. Nevertheless, when samples prepared at subzero temperatures were stored for several hours at room temperature, the methacrylate band completely disappeared from the FTIR spectra, as shown in Fig. S2. The recuperation of mobility of trapped radicals enabled to continue the polymerization to an almost full conversion.

Synthesis of PEG-based macroporous scaffolds

In the presence of water, the system gets more complex and the relationship between the irradiation time and degree of conversion may become not strictly straightforward, although the segregation of the oligomer induced by the freezing process leaves behind an oligomer-rich concentrated phase similar to that of the pure oligomer. In addition, the frozen storage temperature (after ice-templating and during cryo-polymerization) also plays an important role on the final structural characteristics of the freeze-dried materials. This is a direct consequence of the ice crystal lattice evolution due to the recrystallization process, which is the reorganization (at the storage temperature) of the primary formed crystalline structure of ice toward a lower energy structure [36]. In turn, recrystallization involves the enlargement of large ice crystals at the expense of the smallest ones, and this effect strongly depends on the storage temperature. The higher the temperature (nearer 0 °C), the less defined the ice crystal morphology and consequently, the more diffuse the borderline between the ice-rich and oligomer-rich phases generated after the ice-segregation-induced structuring. So, there is a clear compromise between getting, on the one hand, a high degree of conversion after cryo-photopolymerization, and reaching, on the other hand, higher ice integrity, which will define the final porous structure. Accordingly, cryo-photopolymerization of the segregated oligomer (after ice-templating) was carried out in a freezer chamber at −15 °C. This working temperature would allow reaching a high enough conversion to impart a high mechanical strength to the cross-linked structure (necessary for its final manipulation), while promoting and preserving at the same time higher ice integrity. Nevertheless, as occurred with the water-free reactive systems, the recuperation of radical mobility after storage at room temperature allowed attaining full conversion for all tested samples (with aligned or non-aligned pores), without the use of any post-curing additional step. In this way, final formulations were completely devoid of free oligomer, which is of radical importance regarding practical use of these macroporous materials as scaffolds.

Table 1 shows the theoretical and experimental values of bulk densities and porosities of the whole set of cryogels.

For both types of monoliths (with aligned or non-aligned pores), porosities were very close to the initial water content. However, morphologies associated with these porosities were clearly different. The images on the left of Fig. 5 show longitudinal sections of the unidirectionally frozen samples. The images on the right show the corresponding cross sections. Samples evidenced micron-sized aligned channels strongly oriented along the freezing direction. As expected, according to initial oligomer concentrations, monoliths with 80 and 95% porosity showed a

Table 1 Theoretical and experimental values of porosities for monoliths with aligned or non-aligned pores

Sample	Theoretical porosity (%)	Bulk density (g/cm^3)	Experimental porosity (%)
80% Water			
Aligned	80	0.252	78
Non-aligned		0.237	79
95% Water			
Aligned	95	0.080	93
Non-aligned		0.056	95

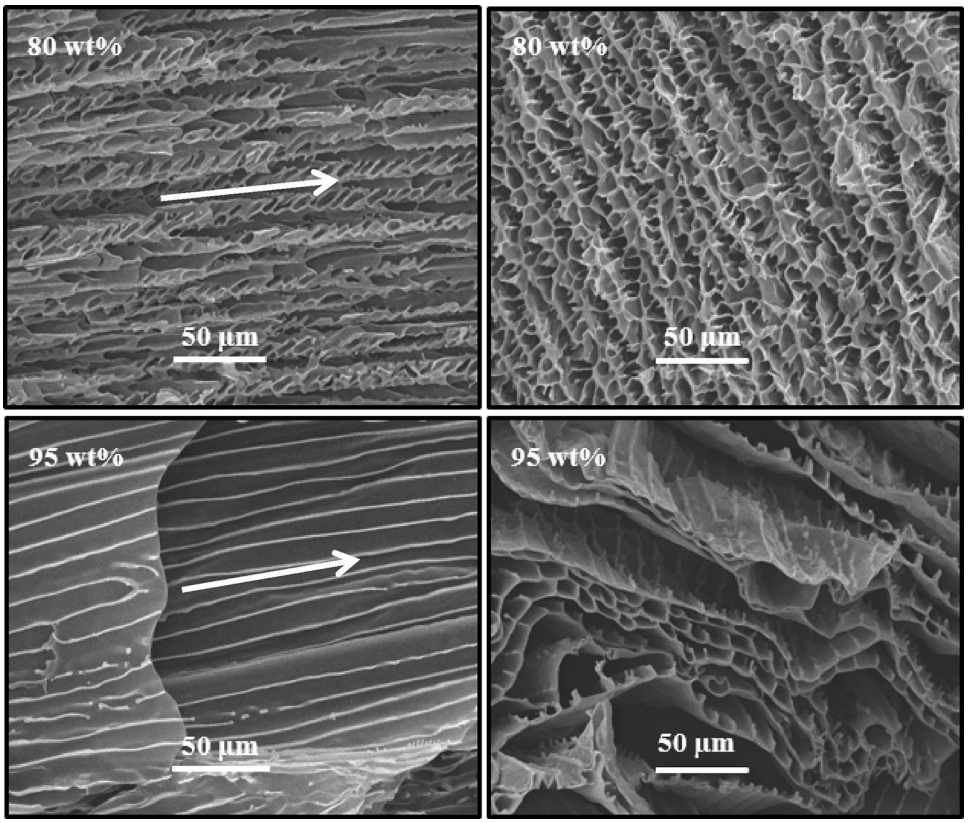

Figure 5 Typical SEM micrographs of monoliths with aligned pores prepared with 80 and 95 wt% water content. The images on the *left* show longitudinal sections of the samples (*arrows* indicate the freezing direction). The images on the *right* show the corresponding cross sections. The water content in the initial solution (wt%) is indicated. *Bars* 50 µm.

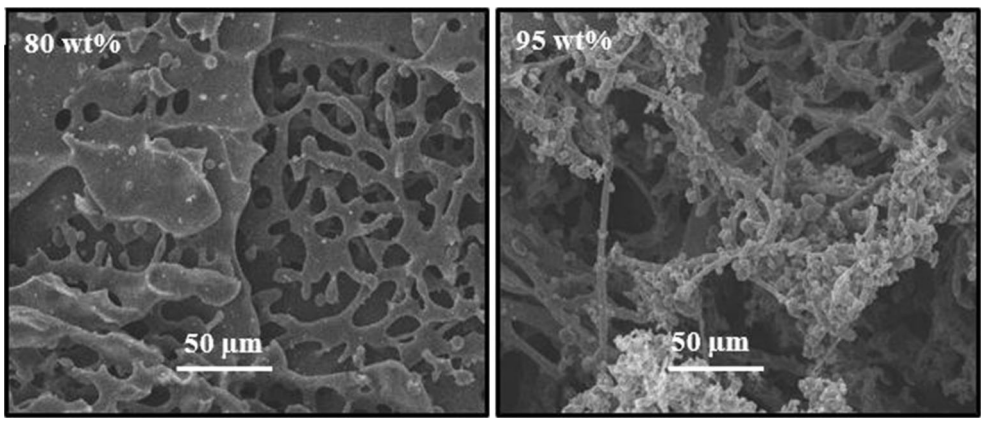

Figure 6 Typical SEM micrographs of monoliths with non-aligned pores prepared with 80 and 95 wt% water content. *Bars* 50 µm.

clear transition from dendrite-like (fish-bone) to smooth (lamellar) pore wall morphologies. These microstructural features are particularly evident in the images of the cross section of both samples.

For the sake of comparison, Fig. 6 shows SEM micrographs of the isotropic monoliths obtained from sudden immersion in liquid nitrogen. The micrographs clearly evidence the presence of randomly oriented macropores for both kinds of samples.

Air permeability of macroporous monoliths

Air permeability was measured for monoliths with 80 and 95% porosity with both aligned and non-aligned

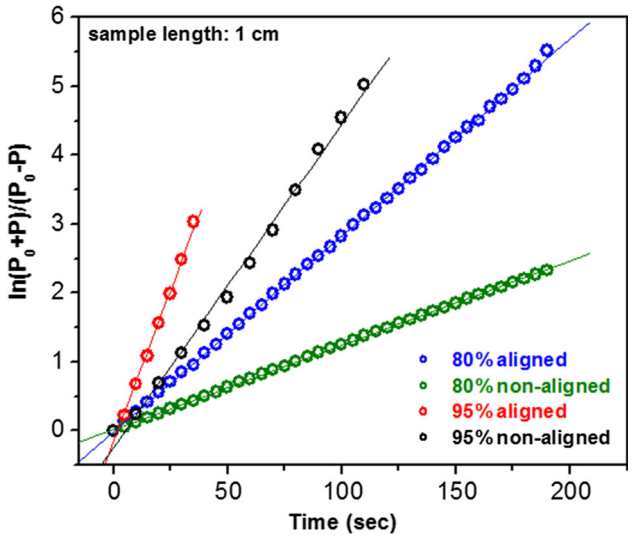

Figure 7 Evolution of pressure with time, plotted in the form of the integrated Darcy's law for monoliths of 1 cm length with 80 and 95% porosity and aligned or non-aligned pores.

pores, employing air as the fluid. The behavior was shown to be strongly dependent on the type of freezing imposed to the samples (Fig. 7).

The results, shown in terms of the linear plots predicted by Eq. (5), confirm the validity of Darcy's law. The influence of the monolith lengths on the resulting permeability values was also investigated for samples with 80% and 95% porosity, using $L = 1$, 1.5, 2 and 2.5 cm. Results are shown in Fig. 8, confirming again the validity of Darcy's law in every case.

Permeability values were calculated from the slopes of the linear plots, and the results are shown in Table 2.

The first significant conclusion arising from this set of values is that, for a particular porosity and pore orientation (aligned or non-aligned), permeability did not show any significant variation with the length of the monolith. Observed variations did not show any definite trend, and all values were comprised in the same range. Thus, the permeability of a monolith with a fixed porosity and pore orientation may be taken as an intrinsic value independent of its length (at least in the investigated range). When screening a set of samples with the same total porosity, pore orientation is demonstrated to play a critical role on permeability. However, the role of the orientation is less marked as porosity increases. Monoliths with non-aligned pores showed a permeability of about 320 mD (average value) for 80% porosity, whereas monoliths with the same porosity but exhibiting aligned pores rendered a permeability three times higher (about 930 mD, average value). Corresponding values for monoliths with 95% porosity ranged between 1260 mD for non-oriented pores and 2360 mD for the anisotropic pore distribution. Results demonstrate that there is a major change in permeability when increasing porosity for the samples processed by a sudden immersion in liquid nitrogen (permeability increased by a factor of 4 as going from 80 to 95% porosity). On the other hand, a more subtle modulation in permeability is possible by aligning pores (the permeability increasing by a factor of 2.5 as going from 80 to 95% porosity). This interestingly suggests that, by selecting aligned or non-aligned samples according to our needs, it would be possible to extend the range and graduate

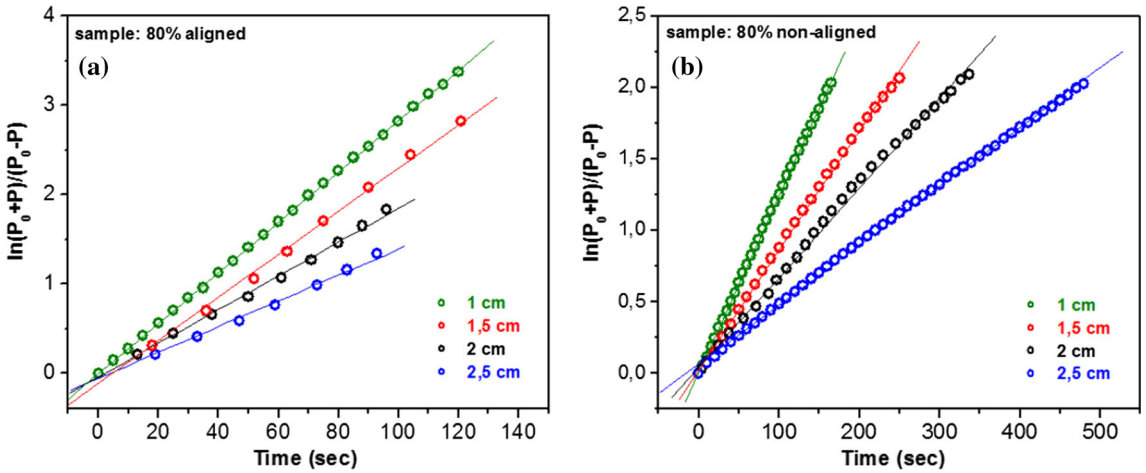

Figure 8 Evolution of pressure with time, plotted in the form of the integrated Darcy's law for monoliths of 80% porosity and lengths of 1, 1.5, 2 and 2.5 cm. **a** Aligned pores and **b** non-aligned pores.

Table 2 Permeability values of monoliths with aligned or non-aligned pores as a function of their lengths and porosities

Sample	Porosity (%)	Sample length (cm)	Permeability (millidarcys)
80% Water			
Non-aligned	80	1	330
		1.5	342
		2	338
		2.5	275
Aligned		1	760
		1.5	970
		2	1013
		2.5	965
95% Water			
Non-aligned	95	1	1260
Aligned		1	2360

the permeability values that can be reached with porous samples. We believe this modulation can be of paramount importance in areas as diverse as tissue engineering, separation science and/or anisotropic membranes, which may require a fine control on permeability changes.

According to the operational conditions used during the unidirectional process, a major control, not only on pore orientation, but also on pore morphologies, led to permeability differences that can be associated with the PEGDMA concentrations in the initial solutions. As concentration increases, so does the viscosity of the solution, leading to both decreased oligomer diffusivity and to a considerable increase in the supercooling of the freezing solution ahead of the growing ice crystals [16]. This induces secondary instabilities perpendicularly to the freezing direction, breaking the initial uniform growing of the ice crystals, evolving toward a branched-like crystal morphology. These effects together are mirrored by the dendrite-like pore morphology created in the sample prepared with the highest oligomer concentration (80% porosity). This feature, typically referred to as a fish-bone morphology, increases considerably the tortuosity of the pore paths along the monolith length and can be used to retard gas streamlines through the porous platform. How much retardation we could produce will depend on processing skills. The possibility of working with a water-soluble monomer/oligomer susceptible of being cryo-photopolymerized could be used as a strategy for pre-polymerizing solutions before ice-templating. This would induce viscosity variations in the initial solutions [32] and, on the light of the obtained results, would allow tuning in a more subtle way the aligned structures and the permeability performance.

Conclusions

Macroporous, highly hydrophilic PEG-based scaffolds were obtained through a simple procedure that involves the cryo-photopolymerization of a commercial precursor with visible light. The proposed strategy presents several advantages that make it a good candidate for scaling-up and real applications, like the use of water as the only solvent, the low energy required for the photopolymerization (sourced by an arrangement of blue LEDs) and the possibility of tuning total porosity and pore morphology by simply changing solution concentration and/or freezing parameters. Results demonstrate that the use of unidirectional freezing strongly increases the permeability of monolithic samples up to values usually required for their use in tissue engineering (higher than 2D). By selecting aligned or non-aligned samples according to our needs, it would be possible to extend the range and graduate the permeability values that can be reached with porous polymeric cross-linked platforms. The findings reported here provide new perspectives on pore design principles toward future scaffolding of polymeric cross-linked matrices.

Acknowledgements

The financial support of the following institutions is gratefully acknowledged: National Research Council

(CONICET), National Agency for the Promotion of Science and Technology (ANPCyT, Argentina, PICT012-2235 and PICT10-1008) and University of Mar del Plata (15/G374).

Compliance with ethical standards

Conflict of interest Authors declare no conflicts of interest for this work.

Electronic supplementary material: The online version of this article (doi:10.1007/s10853-017-1460-4) contains supplementary material, which is available to authorized users.

References

[1] Peppas NA, Huang Y, Torres-Lugo M, Ward JH, Zhang J (2000) Physicochemical foundations and structural design of hydrogels in medicine and biology. Annu Rev Biomed Eng 2:9–29

[2] Hentze H-P, Antonietti M (2002) Porous polymers and resins for biotechnological and biomedical applications. Rev Mol Biotechnol 90:27–53

[3] Plieva FM, Galaev IY, Mattiasson B (2007) Macroporous gels prepared at subzero temperatures as novel materials for chromatography of particulate-containing fluids and cell culture applications. J Sep Sci 30:1657–1671

[4] Petrov P, Petrova E, Tsvetanov CB (2009) UV-assisted synthesis of super-macroporous polymer hydrogels. Polymer 50:1118–1123

[5] Berillo D, Volkova N (2014) Preparation and physicochemical characteristics of cryogel based on gelatin and oxidised dextran. J Mater Sci 49:4855–4868. doi:10.1007/s10853-014-8186-3

[6] Dario Arrua R, Hilder EF (2015) Highly ordered monolithic structures by directional freezing and UV-initiated cryopolymerisation. Evaluation as stationary phases in high performance liquid chromatography. RSC Adv 5:71131–71138

[7] Ertürk G, Mattiasson B (2014) Cryogels-versatile tools in bioseparation. J Chromatogr A 1357:24–35

[8] Zhang H, Chiao M (2015) Anti-fouling coatings of poly(dimethylsiloxane) devices for biological and biomedical applications. J Med Biol Eng 35:143–155

[9] Haryanto Singh D, Han SS, Son JH, Kim SC (2015) Poly(ethylene glycol) dicarboxylate/poly(ethylene oxide) hydrogel film co-crosslinked by electron beam irradiation as an anti-adhesion barrier. Mater Sci Eng, C 46:195–201

[10] Mandy SH (1983) A new primary wound dressing made of polyethylene oxide gel. J Dermatol Surg Oncol 9:153–155

[11] Chatterjee S, Sen Gupta S, Kumaraswamy G (2016) Omniphilic polymeric sponges by ice templating. Chem Mater 28:1823–1831

[12] Ma Q, Cheng H, Fane AG, Wang R, Zhang H (2016) Recent development of advanced materials with special wettability for selective oil/water separation. Small 12:2186–2202

[13] Ge J, Zhao H-Y, Zhu H-W, Huang J, Shi L-A, Yu S-H (2016) Advanced sorbents for oil-spill cleanup: recent advances and future perspectives. Adv Mater 28:10459–10490

[14] Hernandez C, Gawlik N, Goss M, Zhou H, Jeganathan S, Gilbert D, Exner AA (2016) Macroporous acrylamide phantoms improve prediction of in vivo performance of in situ forming implants. J Control Release 243:225–231

[15] Tsujimoto T, Kitagawa T, Yoneda S, Uyama H (2017) Fabrication of amine-functionalized acrylic monoliths via thermally induced phase separation and their application for separation media. J Porous Mater 24:233–239

[16] Deville S (2013) Ice-templating, freeze casting: beyond materials processing. J Mater Res 28:2202–2219

[17] Moghadam MZ, Hassanajili S, Esmaeilzadeh F, Ayatollahi M, Ahmadi M (2017) Formation of porous HPCL/LPCL/HA scaffolds with supercritical CO_2 gas foaming method. J Mech Behav Biomed Mater 69:115–127

[18] Shi B, Shlepr M, Wang JH, Wideman G (2014) New breathable films using a thermoplastic cross-linked starch as a porogen. J Appl Polym Sci. doi:10.1002/app.41016

[19] Kim H, Ahn KH, Lee SJ (2017) Conductive poly(high internal phase emulsion) foams incorporated with polydopamine-coated carbon nanotubes. Polymer 110:187–195

[20] Huang X, Peng Y, Pan J, Zhang W, Zhou W, Zhu H, Liu S (2017) Efficient adsorption of oil by hydrophobic macroporous polymer synthesized with the emulsion template and magnetic particles on the surface. J Appl Polym Sci 134:44731–44739

[21] Ikem VO, Menner A, Horozov TS, Bismarck A (2010) Highly permeable macroporous polymers synthesized from pickering medium and high internal phase emulsion templates. Adv Mater 22:588–3592

[22] Mounesi Rad S, Khorasani MT, Daliri Joupari M (2016) Preparation of HMWCNT/PLLA nanocomposite scaffolds for application in nerve tissue engineering and evaluation of their physical, mechanical and cellular activity properties: nerve tissue engineering, phase separation, multi-walled nanotubes. Polym Adv Technol 27:325–338

[23] Wang Z, Shen X, Han NM, Liu X, Wu Y, Ye W, Kim J-K (2016) Ultralow electrical percolation in graphene aerogel/epoxy composites. Chem Mater 28:6731–6741

[24] Zhao D, Zhu J, Zhu Z, Song G, Wang H (2014) Anisotropic hierarchical porous hydrogels with unique water loss/absorption and mechanical properties. RSC Adv 4:30308–30314

[25] Zhang H, Hussain I, Brust M, Butler MF, Rannard SP, Cooper A (2005) Aligned two- and three-dimensional structures by directional freezing of polymers and nanoparticles. Nat Mater 4:787–793

[26] Dhainaut J, Piana G, Deville S, Guizard C, Klotz M (2014) Freezing-induced ordering of block copolymer micelles. Chem Commun 50:12572–12574

[27] Romeo HE, Hoppe CE, López-Quintela MA, Williams RJJ, Minaberry Y, Jobbágy M (2012) Directional freezing of liquid crystalline systems: from silver nanowire/PVA aqueous dispersions to highly ordered and electrically conductive macroporous scaffolds. J Mater Chem 22:9195–9201

[28] Barrow M, Eltmimi A, Ahmed A, Myers P, Zhang H (2012) Frozen polymerization for aligned porous structures with enhanced mechanical stability, conductivity, and as stationary phase for HPLC. J Mater Chem 22:11615–11620

[29] Ozmen MM, Fu Q, Kim J, Qiao GG (2015) A rapid and facile preparation of novel macroporous silicone-based cryogels via photo-induced thiol–ene click chemistry. Chem Commun 51:17479–17482

[30] Zant E, Blokzijl MM, Grijpma DW (2015) A combinatorial photocrosslinking method for the preparation of porous structures with widely differing properties. Macromol Rapid Commun 36:1902–1909

[31] Seuba J, Deville S, Guizard C, Stevenson AJ (2016) Gas permeability of ice-templated, unidirectional ceramics. Sci Technol Adv Mater 17:313–323

[32] Okaji R, Taki K, Nagamine S, Ohshima M (2012) Preparation of porous honeycomb monolith from UV-curable monomer/dioxane solution via unidirectional freezing and UV irradiation. J Appl Polym Sci 125:2874–2881

[33] Crivello JV, Sangermano M (2001) Visible and long-wavelength photoinitiated cationic polymerization. J Polym Sci A Polym Chem 39:343–356

[34] Russell GT, Napper DH, Gilbert RG (1988) Initiator efficiencies in high-conversion bulk polymerizations. Macromolecules 21:2141–2148

[35] Zhu S, Tian Y, Hamielec AE, Eaton DR (1990) Radical concentrations in free radical copolymerization of MMA/EGDMA. Polymer 31:154–159

[36] Petzold G, Aguilera JM (2009) Ice morphology: fundamentals and technological applications in foods. Food Biophys 4:378–396